Journal of Marine Science and Technology

Volume 24 | Issue 4 Article 10

MONOCULAR IMAGE-BASED LOCAL COLLISION-FREE PATH PLANNING FOR AUTONOMOUS ROBOTS

I-Hsum Li
Department of Information Technology, Lee-Ming Institute of Technology, New Taipei City, Taiwan, R.O.C

Ming-Chang Chen
Department of Electrical Engineering, National Taiwan University of Science and Technology, Taipei, Taiwan, R.O.C.

Wei-Yen Wang
Department of Electrical Engineering, National Taiwan Normal University, Taipei, Taiwan, R.O.C., wywang@ntnu.edu.tw

Shun-Feng Su
Department of Electrical Engineering, National Taiwan University of Science and Technology, Taipei, Taiwan, R.O.C

Yi-Han Chen
Department of Electrical Engineering, National Taiwan Normal University, Taipei, Taiwan, R.O.C

Recommended Citation

Li, I-Hsum; Chen, Ming-Chang; Wang, Wei-Yen; Su, Shun-Feng; and Chen, Yi-Han (2016) "MONOCULAR IMAGE-BASED LOCAL COLLISION-FREE PATH PLANNING FOR AUTONOMOUS ROBOTS," *Journal of Marine Science and Technology*: Vol. 24 : Iss. 4 , Article 10.
DOI: 10.6119/JMST-016-0304-2
Available at: https://jmstt.ntou.edu.tw/journal/vol24/iss4/10

MONOCULAR IMAGE-BASED LOCAL COLLISION-FREE PATH PLANNING FOR AUTONOMOUS ROBOTS

Acknowledgements

This work was supported by the Ministry of Science and Technology, Taiwan, under Grant MOST 104-2221-E-003-024, 104-2221-E-234-001 and 104-2811-E-011-012.

Journal of Marine Science and Technology, Vol. 24, No. 4, pp. 759-770 (2016)
DOI: 10.6119/JMST-016-0304-2

MONOCULAR IMAGE-BASED LOCAL COLLISION-FREE PATH PLANNING FOR AUTONOMOUS ROBOTS

I-Hsum Li[1], Ming-Chang Chen[2], Wei-Yen Wang[3], Shun-Feng Su[2], and Yi-Han Chen[3]

Key words: monocular, local collision-free path planning, autonomous robot.

ABSTRACT

Monocular image-based local collision-free path planning for autonomous robots is presented in this paper. According to a pre-set pair of parallel lines, transformation equations from the image domain to the real world domain are easily defined. Moreover, the distances to obstacles in the robot's visual domain can be estimated. Our proposed method can not only easily identify obstacles and wall edges, but also estimate the distances and plan a collision-free path. Besides, this paper successfully integrates an image processing module with a local collision-free path planning, and also applies them to the collision-free and path planning of a mobile robot. For the proposed local collision-free path planning, the webcam can be located at two different situations: one is setting a webcam located on the ceiling and the other is setting a webcam on a mobile robot. In addition, the measurement method only uses a webcam and four laser projectors. Thus, we do not need to purchase expensive equipment to accomplish the desired results. From the experimental results, it shows that our proposed method can be effectively applied to the local collision-free path planning.

I. INTRODUCTION

Path planning is an important application for autonomous robots (Li et al., 2013; Lee et al., 2014) and it has attracted remarkable attention in recent years. In general, path planning can be formulated as: given the start configuration and the goal configuration in a known/unknown environment and then find a feasible path between the two configurations that do not collide with any obstacles. The path planning problem can be classified into global path planning and local path planning (Sedighi et al., 2004). The global path planning requires complete knowledge about the environment and then generates a collision-free path from the start configuration to the goal configuration according to the mission of the mobile robot. Three common solutions for the global path planning are potential field methods, cell decomposition methods, and probabilistic road map methods (Unsalan 2012; Chen et al., 2013; Li et al., 2014). Being different from the global path planning, the local path planning does not rely on complete environment knowledge but uses sensors to detect obstacles around the robot and seeks a collision-free path in the robot's visual domain (Yasuda and Takai, 2001; Fujimori and Tani, 2002; Wang and Fang, 2009), the range of which is where the robot's sensors can sense. This paper focuses on developing a possible solution for the local collision-free path planning in an unknown environment.

On autonomous control issues, image-based measurement is important but more difficult than device-based measurement. Traditionally, ultrasonic sensors (Han et al., 2009) generate high-frequency sound waves and calculate the time-interval between the sent waves and the returned waves, in order to estimate the distances between the sensor and obstacles. However, the short sensing distance and its sensitiveness to changing environment prevent the local path planning from developing. Diffuse infrared technology (Alessandretti et al., 2007; Wu et al., 2009) is commonly used to detect obstacles, but the short-range signal transmission and line-of-sight requirements limit the growth. Because the laser range finder is a very accurate and quick measurement device, it is widely used in many applications. In Nedevschi et al. (2004), Zhao and Shibasaki (2005), and Subramanian et al. (2006), the laser range finder was used to acquire environment information to identify and avoid obstacles when the robot is in navigation. However, the price is really high. The computer vision (Kim et al., 2005; Fernandes and Neves, 2006; Barawid et al., 2007; Gao et al., 2009; Hsu et al., 2009; Gao et al., 2010; Hsu et al., 2010) has attracted more attention in the field of the real-time path planning because of its reduced prices of devices and richer information compared with other ranger finders. Many vision-based methods have been proposed for distance meas-

Paper submitted 05/26/15; revised 12/09/15; accepted 03/04/16. Author for correspondence: Wei-Yen Wang (e-mail: wywang@ntnu.edu.tw).
[1] Department of Information Technology, Lee-Ming Institute of Technology, New Taipei City, Taiwan, R.O.C.
[2] Department of Electrical Engineering, National Taiwan University of Science and Technology, Taipei, Taiwan, R.O.C.
[3] Department of Electrical Engineering, National Taiwan Normal University, Taipei, Taiwan, R.O.C.

urement (Fernandes and Neves, 2006; Hsu et al., 2009; Gao et al., 2010; Hsu et al., 2010) in the past. Vision based systems are generally equipped with a pair of cameras at different positions on the same horizontal level (Kim et al., 2005). By comparing two captured images of a scene, environment distance information can be obtained in the form of a disparity map, which is inversely proportional to the distance of the object. However, there are some unsolved problems in the dual-camera distance measurement, for examples, the calibration of image planes for dual cameras (Gao et al., 2009) and the depth map calculation (Felzenszwalb and Huttenlocher, 2006; Li et al., 2014). As a result, performance of real-time measurement via the computer-vision-based measurement is generally unsatisfactory. A monocular camera is a lightweight and inexpensive sensor, and it particularly fits the requirements of autonomous robots. Lu et al. (2006) proposed a monocular CCD image-base measuring system for distance and area measurements. The measurement method does not need to store huge image information or use any pattern recognition but simply counts the number of scan line covering targeted objects in the image domain. In Li et al. (2014), distances from a monocular camera to an object is estimated by simple calculations derived from four predefining standard laser spots.

Our proposed image-based local-path planning system executes an obstacle-detection and the local collision-free path planning according to a pre-defined pair of parallel lines. Initially, the parallel lines are built by a known rectangle if the webcam is located on the ceiling or by four laser spots if the webcam and the laser projectors are equipped in the robot. Next, the proposed monocular-image-based distance measurement (MIBDM) can acquire the location of obstacles and wall edges in the captured image and a mapping between the image domain and the real-world domain can transfer the image coordinate into the real-world coordinate. As mentioned above, our proposed method can effectively plan a collision-free path for the mobile robots and, hence, the experimental cost can be evidently reduced.

This paper is divided into five main sections. Section I provides some background information about the image-based obstacle avoidance. Section II outlines the method of the image detection. Design of the monocular-image-based distance measurement system is included in Section III. Section IV presents a number of applications of the path-planning method in the local environment. Finally, we state our conclusions in Section V.

II. IMAGE PROCESSING

The image processing techniques for the proposed local collision-free path planning are discussed in this section. Incorporated techniques include the grayscale transformation, the binarization, the canny edge detection, the morphological image processing, the connected components labeling technique, and the Hough transformation. Whereas the canny edge detection, the connected components labeling, and the Hough transformation are used to discover obstacle and wall edges.

1. Grayscale and Binarization

The grayscale technique converts a captured color image into a black-and-white image with 256 shades of gray. The grayscale $f_g(x,y)$ of the *pixed*(x,y) is defined as

$$f_g(x,y) = 0.299R_{(x,y)} + 0.587G_{(x,y)} + 0.114B_{(x,y)}, \quad (1)$$

where $R_{(x,y)}$, $G_{(x,y)}$, and $B_{(x,y)}$ are RGB colors at the *pixel*(x,y). Then a binary image is produced by the binarization technique, as shown in

$$f_{binary}(x,y) = \begin{cases} 255 & if \quad f_g(x,y) \geq t \\ 0 & else \end{cases}, \quad (2)$$

where t is a threshold value, which is set to 128 in this paper.

2. Canny Edge Detection

An edge is a set of connected pixels that forms a boundary between two disjoint regions. The canny edge detection is a method of segmenting an image into regions of discontinuity and has the advantages of being less sensitive to noise. It is also able to avoid the streaking and provide an edge gradient orientation (Yasuda et al., 2001; Fujimori et al., 2002; Wang et al., 2009; Rashmi et al., 2013).

3. Morphological Image Processing

After completing the canny edge detection, discontinuous edges and noise may happen and possibly damage the process of the local path planning. The aim of morphological image processing is to eliminate noise and reconstruct discontinuous edges to a continuous one.

4. Connected-Components Labeling

The connected-component labeling can detect connected regions on binary images. It scans an image pixel-by-pixel (from top to bottom and left to right) and partitions pixels into one or more regions according to pixel connectivity (for example, 4 connected or 8 connected), which shares the similar pixel intensity values. Once all groups have been determined, each pixel is labeled with a gray level.

5. Hough Transformation (HT)

The HT is an image processing technique for extracting features of particular shapes, such as lines, circles, or ellipses. In this paper, the HT is used to detect wall edges, which can be considered as a line structure inside buildings.

III. MONOCULAR-IMAGE-BASED DISTANCE MEASUREMENT (MIBDM)

The purpose of the local collision-free path planning is to determine a path that a robot must take in order to pass ob-

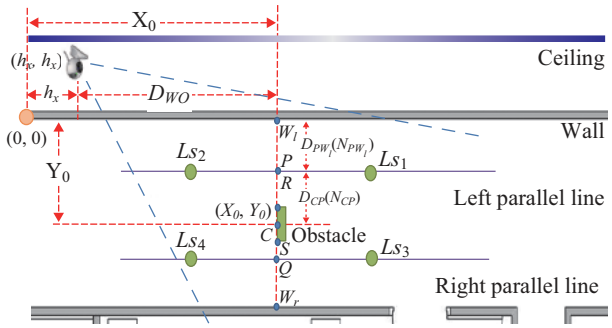

Fig. 2. Structure of virtual indoor environment.

stacles in a local environment. First of all, monocular-image-based distance measurement method is developed for estimating obstacles' depths in the robot's visual domain (Zhu et al., 2011). The idea comes from a sense of how to determine a pixel-to-distance mapping for an object between a captured image and a real environment. In this paper, a pair of parallel lines is formed by four given spots. If the webcam is located on a ceiling, the four given spots can be easily determined by a known dimension rectangle, i.e., a ground tilt; otherwise, if the webcam is equipped on a robot, the spots can be considered as four laser spots from the laser projectors equipped on a robot. Fig. 2 shows the schematic diagram of the proposed MIBDM, where Ls_1, Ls_2, Ls_3, and Ls_4 are the given spots. According to the four spots, a pair of parallel lines Ls_1Ls_2 and Ls_3Ls_4 in the image domain can be formed, and the line equations are respectively described as

$$Ls_1Ls_2 : \frac{y_l - y_1}{y_2 - y_1} = \frac{x_l - x_1}{x_2 - x_1} \tag{3}$$

and

$$Ls_3Ls_4 : \frac{y_r - y_3}{y_4 - y_3} = \frac{x_r - x_3}{x_4 - x_3}, \tag{4}$$

where (x_1, y_1), (x_2, y_2), (x_3, y_3), and (x_4, y_4) are the image coordinates of the points Ls_1, Ls_2, Ls_3, and Ls_4. Note that these four points can be found because of the use of the image processing techniques in Section II. The image coordinate (x_l, y_l) could be any point laying in line Ls_1Ls_2 and the image coordinate (x_r, y_r) is any point laying in line Ls_3Ls_4. The pixel difference(s) N_{QP} between the points Q and P is calculated by

$$N_{QP} = Ls_3Ls_4(y_r) - Ls_1Ls_2(y_l) = x_r - x_l. \tag{5}$$

If the points Ls_1 and Ls_3 are in the same horizontal scan line, the coordinate y_r equals to y_l and the distances between any two points lying in the same horizontal scan line can be

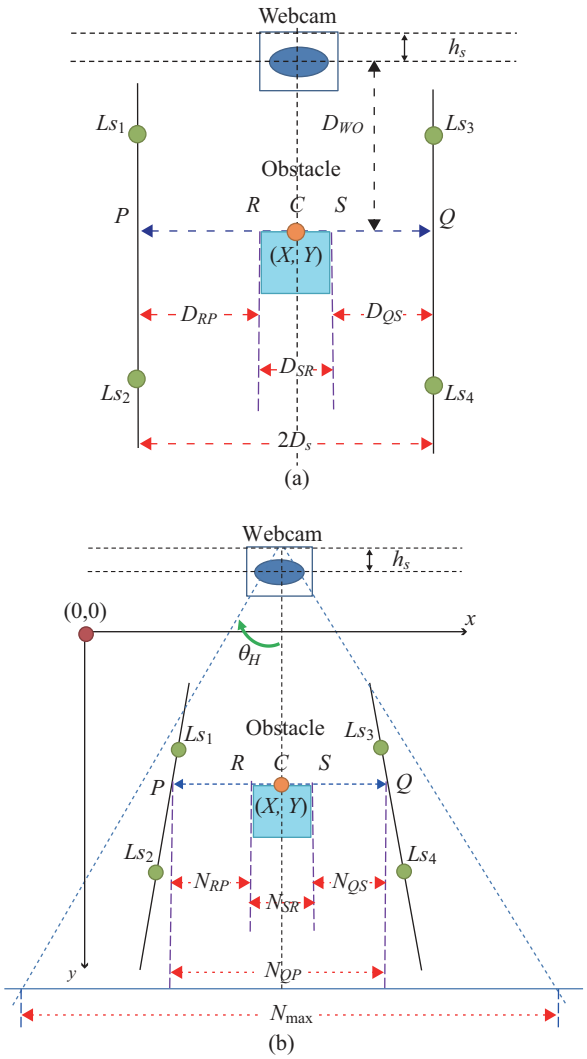

Fig. 1. Structure of MIBDM (a) bird's-eyes view; (b) captured image.

calculated, as shown in Fig. 1. Therefore, the width D_{SR} of the obstacle is shown as

$$D_{SR} = \frac{N_{SR}}{N_{QP}} \times 2D_s, \tag{6}$$

where S and R are two points in the same horizontal scan line, and D_s is a half of distance between the parallel lines. Otherwise, the distance D_{WO} between the obstacle and the webcam can be calculated as Eq. (7) by the simple

$$D_{WO} = \frac{N_{\max}}{N_{QP}} \times D_s \times \cot\theta_H - h_s, \tag{7}$$

where θ_H is the horizontal view angle, h_s is the position of optical origin, $N_{\max}$ is the maximal pixel width in a horizontal scan line of the image. Then the proposed MIBDM can cal-

culate the distances between any two points in the image domain. Hence, the depth and the width of obstacles in a robot's visual domain can be easily obtained.

IV. LOCAL COLLISION-FREE PATH PLANNING

1. Webcam Located on a Ceiling

Fig. 2 shows the set-up of a webcam located on a ceiling. In this experimental environment, the locations of the webcam and the wall edges are given and the parallel lines can be easily formed by choosing the corners of a tile as the four points (Ls_i $i = 1, \ldots, 4$). Note that the four points should be closer in reality; for clarity, we magnify the intervals between the points. In the experimental environment, (X_0, Y_0) is the coordinate of the obstacle and (h_x, h_y) is the coordinate of the camera.

Clearly, the coordinate (X_0, Y_0) of the obstacle is expressed as

$$\begin{cases} X_0 = h_x + D_{WO} \\ Y_0 = D_{PW_l} + D_{CP} \end{cases}, \tag{8}$$

where D_{WO} represents the distance from the webcam to the obstacle, D_{PW_l} represents the distance from the left wall edge to the left parallel line, and D_{CP} represents the distance from the left parallel line to the obstacle. According to the proposed MIBDM, the distances D_{WO}, D_{PW_l}, and D_{CP} are calculated by

$$D_{WO} = \frac{N_{\max}}{N_{QP}} \times D_s \times \cot\theta_H - h_s, \tag{9}$$

$$D_{PW_l} = \frac{N_{PW_l}}{N_{QP}} \times 2D_s, \tag{10}$$

and

$$D_{CP} = \frac{N_{CP}}{N_{QP}} \times 2D_s, \tag{11}$$

where N_{PW_l} is the number of pixel from the left wall edge to the left parallel line in the image domain and N_{CP} is the number of pixel from the left parallel line to the obstacle in the image domain. The points W_l, P, R, and C are staying the same scan line and the points R, and C can be found by using the image processing techniques, as shown Fig. 1; hence, N_{PW_l} and N_{CP} can be calculated. The robot's visual domain is assumed to be three-fifths of the captured image (the part near to the robot). Fig. 3 shows the block diagram of the proposed local collision-free path planning and Fig. 4 gives an example to show the procedures, in which three obstacles are within the robot's visual domain. The flowchart of the path-planning strategy has been included in the revised manuscript, as shown in Fig. 5. In Fig. 5, both $D_{C_A W_{la}}$ and $D_{W_{ra} C_A}$ represent as the distance between an obstacle and a wall, D_H stands for the width of the robot, and $point_i$ represents the center of $D_{C_A W_{la}}$ or $D_{W_{ra} C_A}$. The steps of the local collision-free path planning can be expressed as,

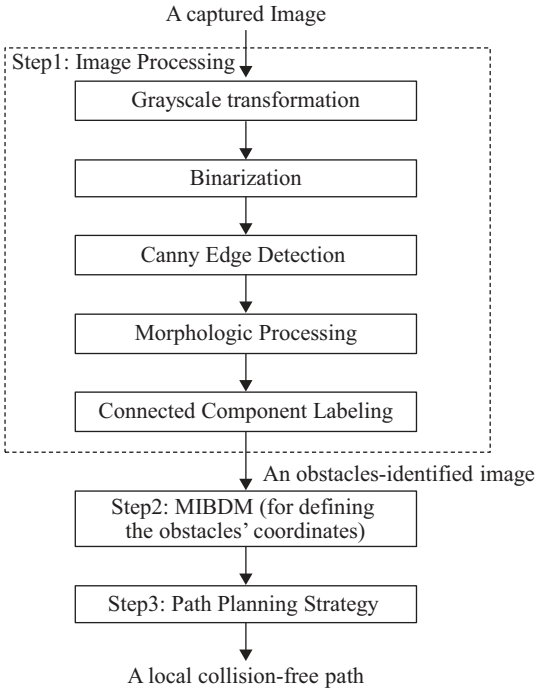

Fig. 3. Procedures of the local collision-free path planning (the webcam is located on the ceiling).

Step 1: Image Processing

Locate the obstacles and find the needed information, such as the coordinates of W_{la}, W_{lb}, W_{lc}, W_{ra}, W_{rb}, W_{rc}, C_A, C_B, and C_C by using the image processing techniques.

Step 2: Calculations of Obstacle Coordinate

Calculate the distances of $D_{C_A W_{la}}$, $D_{C_B W_{lb}}$, $D_{C_C W_{lc}}$, $D_{W_{ra} C_A}$, $D_{W_{rb} C_B}$, $D_{W_{rc} C_C}$, D_{WO_A}, D_{WO_B}, D_{WO_C} using the proposed MIBDM.

Step 3: Path Planning Strategy

Decide the collision-free path. For the first obstacle, because $D_{C_A W_{la}} > D_{W_{ra} C_A}$ and $D_{C_A W_{la}} > D_H$, the robot moves toward the $Point\,1 = (X_{0A}, \frac{Y_{WA_1} + Y_{0A}}{2}) = (X_1, Y_1)$ and the path is set to $Path_{01}$. Similar to the procedures of choosing $Path_{01}$, $Path_{12}$, $Path_{23}$, and $Path_{34}$ are found. Connect these paths

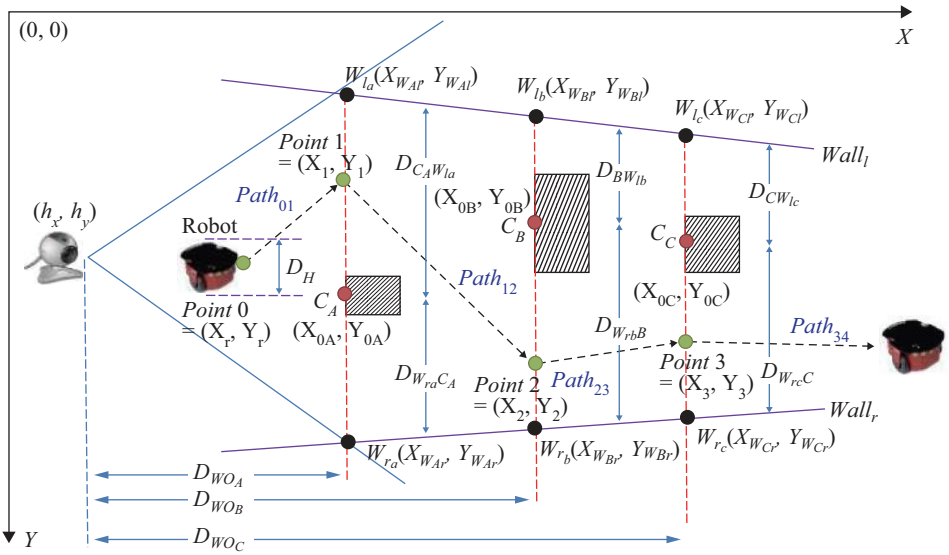

Fig. 4. Diagram of the proposed collision-free path planning method.

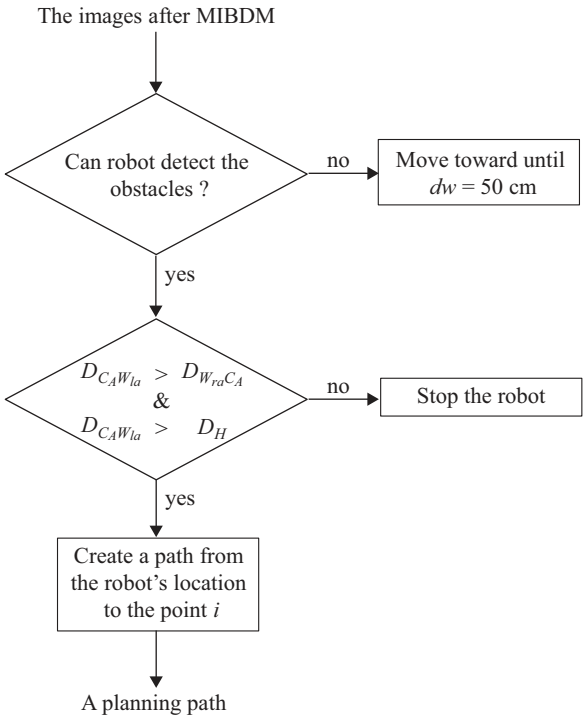

Fig. 5. Flowchart of the path-planning strategy.

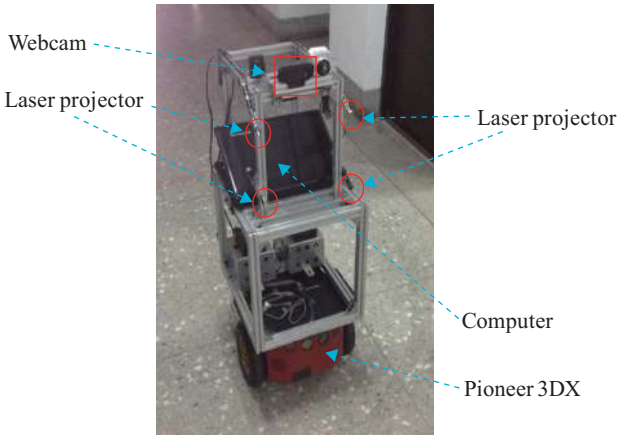

Fig. 6. Applied robot for the local collision-free path planning.

and the local collision-free path $Path_{01} \rightarrow Path_{12} \rightarrow Path_{23} \rightarrow Path_{34}$ is then established.

2. Robot Equipped with Webcam

Since the robot is equipped with a webcam, its visual domain is changed over time, and because the camera coordinates (h_x, h_y) is unknown, Eq. (8) cannot calculate the coordinates of obstacles. Fig. 6 shows the Pioneer 3DX robot used in the experiments and equipped with a webcam, four laser projectors as well as 500-tick encoders to provide information for an odometry. In this case, the four laser projectors project four red spots on the floor as the needed points $Ls_i (i = 1, \ldots, 4)$, and a pair of parallel lines is established. Note that in this hardware configuration, vibration may lead to the problem of building the precise parallel lines when the robot is moving. Therefore, in this experiment the parallel line is built before the robot begins to move. Moreover, the location (X_r, Y_r) and heading angular θ of the robot are estimated by the odometer. Fig. 7 shows the block diagram of the local collision-free path planning in which the webcam is equipped on the robot. The Hough transformation is applied to detect the location of the wall edges, while the morphologic processing and the connected component labeling techniques are applied to find the boundaries of the obstacles.

The detailed steps of the local collision-free path planning are:

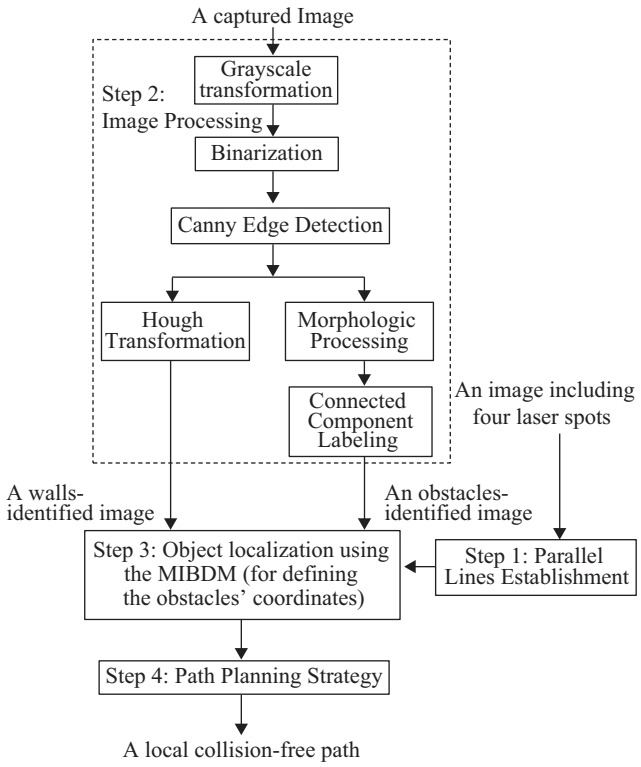

Fig. 7. Block diagram of the local collision-free path planning (the webcam is equipped on the robot).

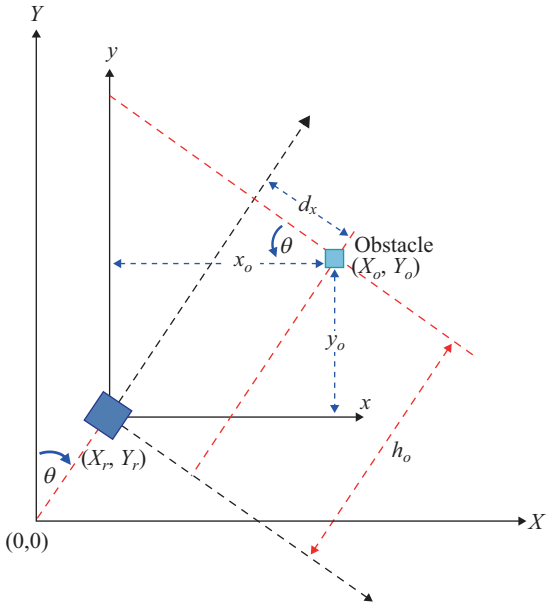

Fig. 8. Calculation of the map coordinates of an obstacle.

Step1: Parallel Lines Establishment

The four laser projectors project four red spots on the floor, and the robot locates the red spots in the pre-set regions of interest (ROIs). Since the configuration of the four laser projectors is known, i.e., the projectors' heights and the heading angles as well as their intervals, ROIs could easily be set up.

Step 2: Image Processing

Locate the obstacles and the wall edges, and find the needed information for Eqs. (3)-(7) by using the image processing techniques.

Step 3: Object Localization

This step is to calculate the map coordinates of the wall edges and the obstacles. Eqs. (12) and (13) show the calculation of the relative map coordinates (x_o, y_o) from the location of the robot, as shown in Fig. 8, in which θ represents the heading angle and is given by the odometer, h_o is the distance from the robot to an obstacle, and d_x is the distance from the obstacle to the boundary of the robot's image domain. To find (x_o, y_o), the equations of the relative coordinate are expressed as

$$x_o = h_o \sin\theta + d_x \cos\theta, \tag{12}$$

$$y_o = h_o \sin\theta + d_x \cos\theta, \tag{13}$$

Then, the map coordinate of the obstacles is

$$X_o = X_r + x_o, \tag{14}$$

and

$$Y_o = Y_r + y_o, \tag{15}$$

where the coordinate (X_r, Y_r) is the coordinate of the robot, which is also given by the odometer.

Step 4: Path Planning Strategy

Decide the collision-free path when change of the captured image is detected. In this example, as shown in Fig. 9, there are three obstacles in the indoor environment and four situations should be taken into account for the local collision-free path planning.

Situation 1 (Fig. 9(a)):

The robot faces three obstacles, but the visual domain only converts first two obstacles. In this case $D_{C_A W_{la}} > D_{W_{ra} C_A}$ and $D_{C_A W_{la}} > D_H$, so the robot moves toward the $Point\,1 = (X_1, Y_1) = (X_{0A}, (Y_{WA_1} + Y_{0A})/2)$ and the path is set to Path_{01}. Similar to the procedures of choosing $Path_{01}$, $Path_{12}$ can be found, and $Path_{23}$ is set to be parallel to the wall edge because the robot detects nothing behind the second obstacle in the robot's visual domain. Connect these paths and the local collision-free path $Path_{01} \rightarrow Path_{12} \rightarrow Path_{23}$ is then established.

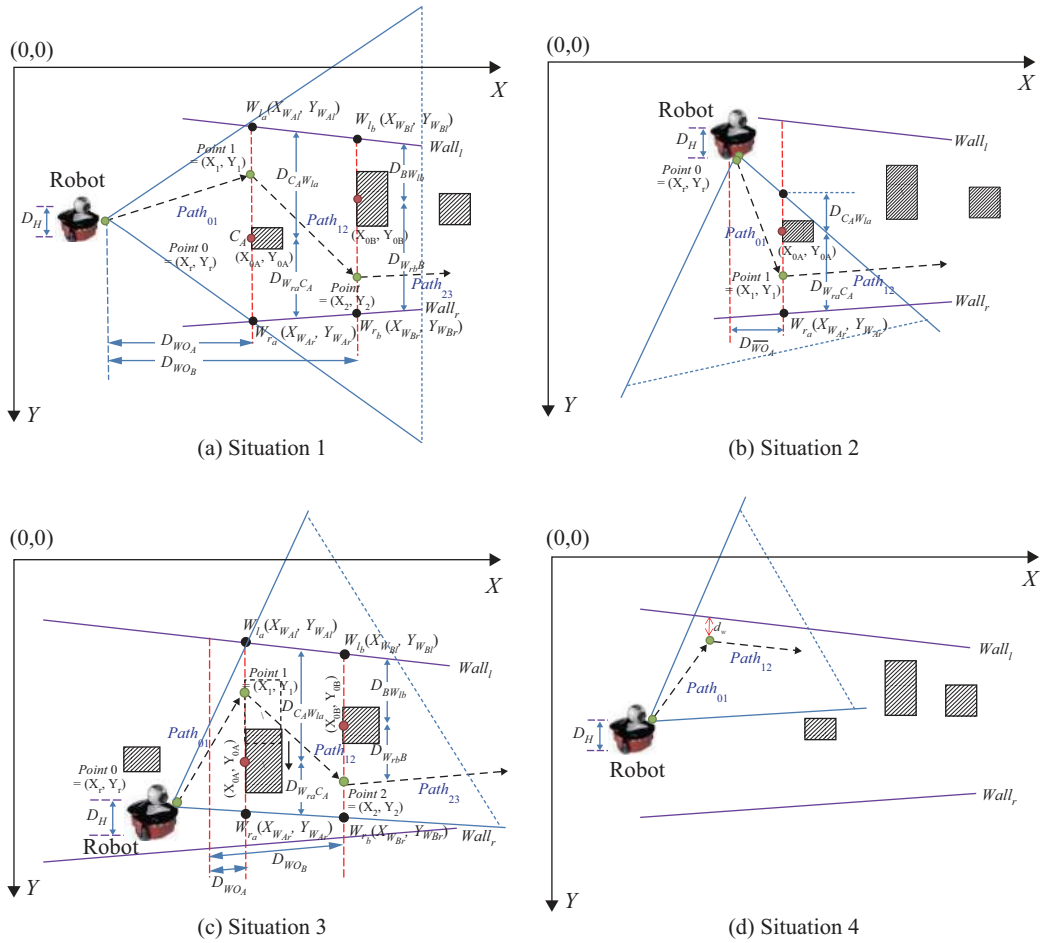

Fig. 9. Diagram of the proposed collision-free path planning method (robot equipped with the webcam).

Situation 2 (Fig. 9 (b)):

The robot only sees one obstacle and the wall edge $Wall_r$. In this case $D_{W_{ra}C_A} > D_{C_AW_{la}}$ and $D_{W_{ra}C_A} > D_H$, so the robot moves toward the $Path\ 1 = (X_1, Y_1) = (X_{0A}, (Y_{WA_1} + Y_{0A})/2)$ and the path is set to $Path_{01}$. $Path_{12}$ is set to be parallel to the wall edge because the robot detects nothing behind the first obstacle in the robot's visual domain. Connect these paths and the local collision-free path $Path_{01} \rightarrow Path_{12}$ is then established. Note that the point W_{la} is set to the point on the boundary of the image instead of choosing the point on the wall edge $Wall_l$, because for safety reason, we should only consider the robot's visual domain.

Situation 3 (Fig. 9 (c)):

The robot sees two obstacles and the first obstacle moves down. In this case $D_{C_AW_{la}} > D_{W_{ra}C_A}$ and $D_{C_AW_{la}} > D_H$, and the robot moves toward the $Point\ 1 = (X_1, Y_1) = (X_{0A}, (Y_{WA_1} + Y_{0A})/2)$ and the path is set to $Path_{01}$. Similar to the procedures of choosing $Path_{01}$, $Path_{12}$ can be found, and $Path_{23}$ is set to be parallel to the wall edge because the robot detect nothing behind the second obstacle in the robot's visual domain. Connect these paths and the local collision-free path $Path_{01} \rightarrow Path_{12} \rightarrow Path_{23}$ is then established.

Situation 4 (Fig. 9 (d)):

The robot sees nothing in the visual domain but the wall edge $Wall_l$. The robot moves toward the wall edge until it is $d_w = 50$ cm apart, turns right, and then continues along the wall edge.

V. EXPERIMENTAL RESULTS

The Pioneer 3DX robot and a laptop with a core i5 CPU and 4G RAM are used in those experiments. In the robot, the used webcam can provide 640*480 resolution images (around 20 fps). The desired location of the webcam in the local collision-free path planning is to cover as bigger area as possible. In Experiment 1, the webcam is located on 280 cm high, and In Experiment 2, the hallway is 150 cm wide and 500 cm long. The planned path data is transmitted to the server with USB 2.0 interface in Experiment.

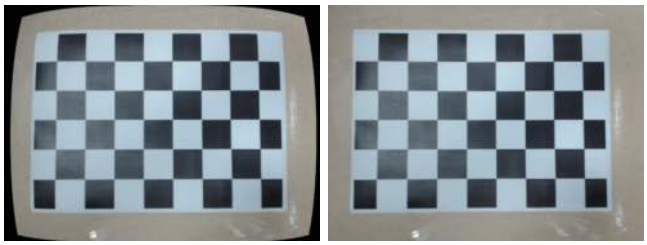

(a) (b)

Fig. 10. Calibration procedure for the webcam Image (a). Captured image by webcam (b). Calibration produced for the webcam.

The captured images might produce distortion phenomenon in the image corner/edge, and the location of obstacles and wall edges could lose the accuracy of image measurement. Thus, camera calibration is very important in the localization. OpenCV has been taken into account the radial and tangential factors for the image distortion problem, where the radial factors are calculated by the following equations,

$$x_{corrected} = x(1 + k_1 r^2 + k_2 r^4 + k_3 r^6) \tag{16}$$

and

$$y_{corrected} = y(1 + k_1 r^2 + k_2 r^4 + k_3 r^6), \tag{17}$$

where r is the rotational variables. k_1, k_2, and k_3 are radial coefficients. Then the tangential distortion is corrected via the equations as following:

$$x_{corrected} = x + [2p_1 xy + p_2(r^2 + 2x^2)] \tag{18}$$

and

$$y_{corrected} = y + [p_1(r^2 + 2y^2) + 2p_2 xy], \tag{19}$$

where p_1 and p_2 are tangential distortion coefficients. The pixel (x, y) is the image coordinate in the captured image and $(x_{corrected}, y_{corrected})$ is the image coordinate in the output image. The distortion coefficient vector can be represented as vector $c_{di} = [k_1 \ k_2 \ p_1 \ p_2 \ k_3]$. Moreover, the unit conversion can be represented as a camera matrix

$$\begin{bmatrix} x \\ y \\ w \end{bmatrix} = \begin{bmatrix} f_x & 0 & c_x \\ 0 & f_y & c_y \\ 0 & 0 & 1 \end{bmatrix} \begin{bmatrix} x \\ y \\ z \end{bmatrix} \tag{20}$$

where w is explained by the use of homography coordinate system (and $w = z$), f_x and f_y are the camera focal length, and c_x and c_y are the optical centers expressed in pixels coordinates. After calculating the camera matrix and the distortion coefficients c_{di}, the OpenCV functions *initUndistortRectifyMap*() and the *remap*() calibrate the distorted images. Fig. 10(a) shows the images before the calibration on the three webcams are produced, and Fig. 10(b) shows the images after the calibration. In our experimental environments, the distortion coefficient vectors are expressed as

(a) (b)

Fig. 11. (a) Set-up of the webcam, (b) webcam's visual domain.

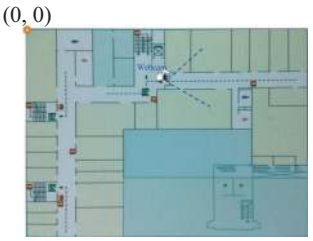

Fig. 12. Set-up of the experimental environment.

$$c_d = [0.2460 \ \ -1.8737 \ \ -0.0023 \ \ -0.0043 \ \ 5.4119] \tag{21}$$

and the camera conversion matrix is

$$\begin{bmatrix} x \\ y \\ w \end{bmatrix} = \begin{bmatrix} 598.36 & 0 & 318 \\ 0 & 600.76 & 264.19 \\ 0 & 0 & 1 \end{bmatrix} \begin{bmatrix} x \\ y \\ z \end{bmatrix}. \tag{22}$$

Experiment 1:

The webcam is located on a ceiling in this experiment, as shown in Fig. 11(a), while the visual domain is set to be three-fifths of the image domain in Fig. 11(b). Fig. 12 shows the experimental environment, in which the left-top corner is set to the origin and the area covered by the blue dash line is the hallway where the robot has to move through.

The aim of the example is to plan a local collision-free path for the Pioneer 3DX robot in an indoor environment. In order to identify the location of the obstacle, this paper utilizes image processing techniques such as the grayscale, the medium filter, the morphologic, the canny edge detector, the Hough transform, and the connected component labeling to recognize the obstacles. In Experiment 1, the webcams directly connect to the server with USB 2.0 interface. Limited by the USB 2.0 transfer rate (around 25 MB/sec in our devices), the resolutions of the captured images is chosen as 640*480 dpi. Then,

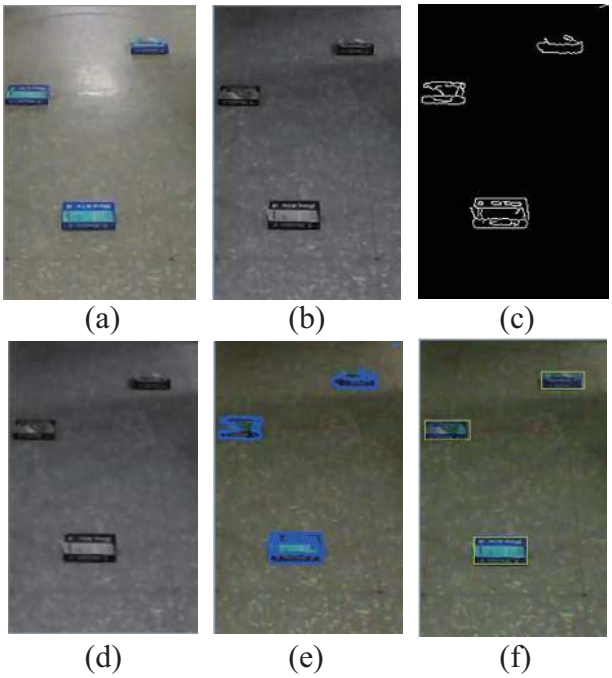

Fig. 13. (a) ROI image, (b) Grayscale image, (c) Canny edge detection image, (d) Morphological processed image, (e) Connected component labeling, and (f) Image of framing obstacles.

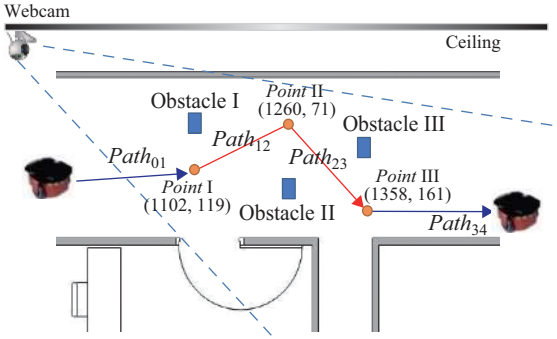

Fig. 14. Actual coordinates on two-dimensional map.

we frame the portion included hallway in the image as ROI and filter images outside ROI to decrease complicated environment images. In this experimental environment, the A4 size paper bags are set as obstacles, as shown in Fig. 13(a). First, the robot captures an image, shown in Fig. 13(a). Then, transfer the image to the grayscale intensity image, shown in Fig. 13(b). After processing the grayscale image by the canny edge detection as shown in Fig. 13(c), using the morphologic processing to eliminate unnecessary noises as shown in Fig. 13(d), and the contours of obstacles are shaped like a rectangle, shown in Fig. 13(e). The midpoint of the bottom line on the rectangle is considered to be the obstacle coordinate in the image in Fig. 13(f). Thus, the coordinates of the obstacles in the image-domain can be obtained, and the coordinates of the obstacles in the real-world domain can be calculated by using the proposed MIBDM.

Table 1. Measurement error using the proposed method.

	Ground truth (cm)	Relative map coordinate (cm)	Error (cm)	Error (%)
Point I	(1104,120)	(1102,119)	2.1	0.2
Point II	(1252,73)	(1260,71)	7.87	0.6
Point III	(1342,163)	(1358,161)	15.6	1.2

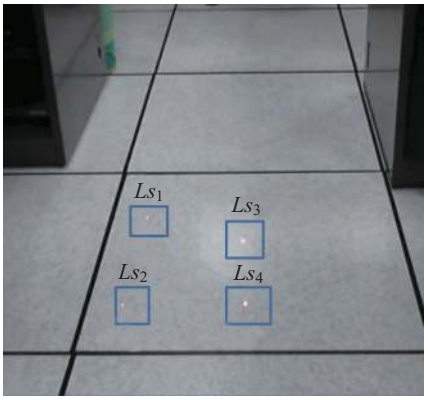

Fig. 15. Region of interest of four laser projectors.

Fig. 14 shows the planned local collision-free path for the Pioneer 3DX robot, in which the points $Point_i (i = \mathrm{I}, \ldots, \mathrm{III})$ are measured by our proposed method and the path could be set to $path_{01} \rightarrow path_{12} \rightarrow path_{23} \rightarrow path_{34}$. The coordinates of the points $Point_i (i = \mathrm{I}, \ldots, \mathrm{III})$ are shown in Table 1, where the error and percent error formula used in Table 1 are shown as

$$error(cm) = \left| \sqrt{(x_m^2 + y_m^2)} - \sqrt{(x_r^2 + y_r^2)} \right|, \tag{23}$$

$$error(\%) = \left| \frac{\sqrt{(x_m - x_r)^2 + (y_m - y_r)^2}}{\sqrt{x_r^2 + y_r^2}} \right|, \tag{24}$$

where (x_r, y_r) is the ground truth coordinate, and (x_m, y_m) is the measured coordinate of the points. The experimental results indicate that if the obstacles are far from the robot, i.e., Obstacle III, measurement error increases because of poor image quality.

Experiment 2:

As the robot is equipped with the webcam, shown in Fig. 6, the robot's visual domain and coordinate will change over time. Thus, coordinates of the obstacles cannot be directly calculated by the Eq. (10). In this experiment, we first build the parallel lines with four given laser spots $Ls_i (i = 1, \ldots, 4)$, and these spots are projected by the equipped laser projectors on the robot shown in Fig. 15. Note that this process mechanism can be performed on any flat floor. There are three obstacles

Fig. 16. Identification results of the edge of wall edges.

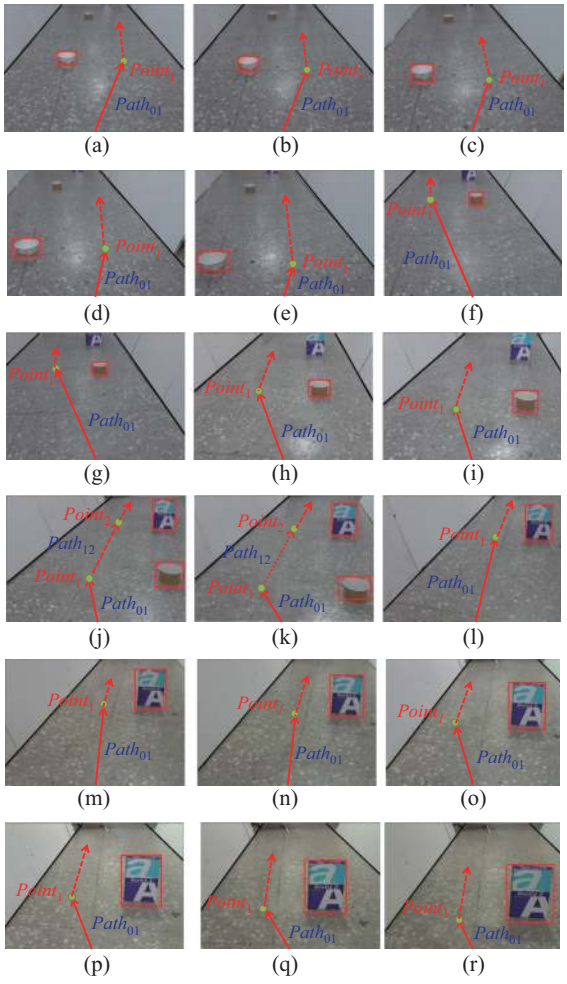

Fig. 17. Local collision-free path planning in a moving obstacle environment.

in the experimental environment and one of them appeared at the beginning of the robot's visual domain. Fig. 16 shows that the indoor environment and the obstacle in the robot's visual domain are detected by using our proposed image processing techniques. When the robot starts moving, the first obstacle is within the visual domain and the robot decides to move to the $point_1 = (25,178)$ following the path $path_{01}$, as shown in Figs. 17(a)-(e). In this duration, the obstacles stay in the same locations. As soon as the robot reaches the $point_1 = (25,178)$, the second obstacle moves right behind the third obstacle and is in the robot's visual domain. The robot decides to move to the $point_1 = (2,125)$ and follow the path $path_{01}$, as shown in Figs. 17(f) and (i). In Figs. 17(j) and (k), there are two obstacles in the robot's visual domain; therefore, the collision-free path $path_{01} \rightarrow path_{12}$ can be found. When the robot reaches the $point_1 = (26,251)$ in Fig. 17(j), the third obstacle is only one left in the visual domain; the robot detects the third one and plans a collision-free path $path_{12}$ to go through the obstacle, as shown in the Figs. 17(l)-(r). The mesauring results are shown in Table 2, in which the error function is also defined as (25) and (26). The experimental results show that if the obstacles are far away from the robot, the measurement error increases because of poor image quality. Thus, if the obstacles are located within the webcam's visual domain (three-fifths of the captured image), the measurement error range is between 0.6 cm and 5.32 cm. On the contrary, if the obstacles are not located in the webcam's visual domain, our proposed method only provides directions of movement to the robot. In order to show the obstacles-avoiding process clearly, the schematic diagram of local collision-free path panning has been included in the revised manuscript, as shown in Fig. 18. Moreover, in the moving process, the accuracy of measurement will be improved as shown in Table 2.

Table 2. Results of actual locations and measuring locations in a moving obstacle environment.

Fig. 17	Measurement point	Ground truth (cm)	Relative map coordinate (cm)	Error (cm)	Error (%)
(a)	$Point_1$	(25, 178)	(25.52, 182.17)	4.2	2.28
(b)	$Point_1$	(17, 164)	(19.1, 168.06)	4.26	2.7
(c)	$Point_1$	(12, 152)	(12.95, 153.01)	1.08	0.9
(d)	$Point_1$	(4, 140)	(6.55, 140.09)	0.19	1.82
(e)	$Point_1$	(2, 125)	(4.97, 122.97)	1.95	2.9
(f)	$Point_1$	(-53, 230)	(-50.30, 255.55)	24.42	10.89
(g)	$Point_1$	(-44, 210)	(-45.06, 233.38)	23.13	10.9
(h)	$Point_1$	(-24, 171)	(-21.61, 176.47)	5.11	3.46
(i)	$Point_1$	(-12, 150)	(-12.55, 150.56)	0.6	0.52
(j)	$Point_1$	(-8, 138)	(-6.48, 135.05)	3.02	2.4
(j)	$Point_1$	(26, 251)	(25.07, 261.47)	10.3	4.16
(k)	$Point_1$	(-14, 127)	(-11.55, 121.90)	5.32	4.4
(k)	$Point_1$	(20, 229)	(19.21, 238.31)	9.21	4.06
(l)	$Point_1$	(18, 210)	(21.27, 218.90)	9.16	4.45
(m)	$Point_1$	(7, 194)	(7.54, 206.12)	12.13	5.17
(n)	$Point_1$	(7, 176)	(6.11, 186.38)	10.34	5.9
(o)	$Point_1$	(-18, 160)	(-14.26, 163.67)	3.28	3.24
(p)	$Point_1$	(-15, 147)	(-13.75, 145.14)	1.97	1.51
(q)	$Point_1$	(-18, 138)	(-16.54, 135.05)	3.1	2.37
(r)	$Point_1$	(-9, 128)	(-9.64, 125.15)	2.79	2.22

In the experiments, the measured locations of obstacles are shown in Table 1 and Table 2. In these two tables, we can see

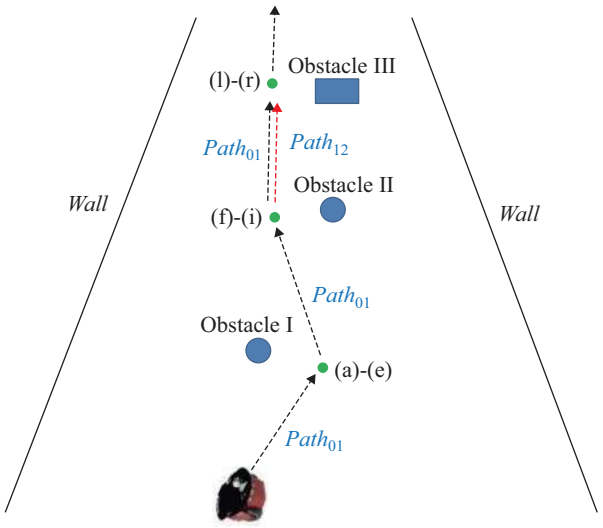

Fig. 18. Schematic diagram of local collision-free path planning.

that most of the error is under 5%. The robot moves on the floor of a building; that is, the floor property is almost unchangeable. Therefore, the first detection process can be completed at the very beginning; this means that we can choose a relative perfect environment (flat floor, sufficient light, and no reflection effect) for the robot to detect the four laser marks. Also, this detection process can be done by manual operation, in order to increase the detection accuracy of the four spots. Hence, lighting conditions or reflection of laser can be reasonable ignored in our case. We should consider the lighting condition and floor property in the future if the robot stays and moves in complex environment.

VI. CONCLUSION

This paper combines obstacle detection with the monocular-image-based distance measurement (MIBDM), and applies them to the local collision-free path planning. The location of obstacles can easily be recognized via our proposed image processing method. Since the measured pixel values are hardly used in the actual environment, the MIBDM is adapted to convert the measured pixel values into the actual distance. According to both the MIBDM and the local collision-free path planning algorithm, the Pioneer 3DX robot can obtain an appropriate moving path. In addition, the proposed method is inexpensive and requires little time in establishing an experiment environment. Finally, the results presented in this paper indicate that our proposed path planning can be effectively used in the known/unknown environments.

ACKNOWLEDGMENT

This work was supported by the Ministry of Science and Technology, Taiwan, under Grant MOST 104-2221-E-003-024, 104-2221-E-234-001 and 104-2811-E-011-012.

REFERENCES

Alessandretti, G., A. Broggi and P. Cerri (2007). Vehicle and guard rail detection using radar and vision data fusion. IEEE Trans. on Intelligent Transportation Systems 8, 95-105.

Barawid Jr., O. C., A. Mizushima, K. Ishii and N. Noguchi (2007). Development of an autonomous navigation system using a two-dimensional laser scanner in an orchard application. Biosystems Engineering 96, 139-149.

Chen, Y. H., M. C. Chen, I-H. Li, W. Y. Wang and S. F. Su (2013). Image-Based Obstacle Avoidance and Path-Planning System. Proceeding of IEEE International Conference on System Science and Engineering, Budapest, Hungary, 205-209.

Felzenszwalb, P. F. and D. P. Huttenlocher (2006). Efficient belief propagation for early vision. Int. Journal Computer Vision 70(1), 41-54.

Fernandes, J. C. and J. A. B. Neves (2006). Angle invariance for distance measurements using a single camera. Proceeding of IEEE International Symposium on Industrial Electronics, Montreal, QC, Canada, 676-680.

Fujimori, A. and S. Tani (2002). A navigation of mobile robots with collision avoidance for moving obstacles. Proceeding of IEEE International Conference on Industrial Technology, 1-6.

Gao, Z. W., W. K. Lin, Y. S. Shen, C. Y. Lin and C. C. Chang (2009). Stereo correspondence based on rotation invariant correlation. Proceeding of IEEE International Symposium on Circuits and Systems, 1489-1492.

Gao, Z. W., W. K. Lin, Y. S. Shen, C. Y. Lin and W. C. Kao (2010). Design of signal processing pipeline for stereoscopic camera. IEEE Trans. on Consumer Electronics 56(2), 324-331.

Han, S. M., S.-K. Park, J.-H. Jung and K.-W. Lee (2009). Mobile robot navigation by circular path planning algorithm using camera and ultrasonic sensor. Proceeding of IEEE International Symposium on Industrial Electronics, Korea, 1749-1754.

Hsu, C. C., M. C. Lu, W. Y. Wang and Y.-Y. Lu (2009). Distance measurement based on pixel variation of CCD images. ISA Trans. 48, 389-395.

Hsu, C. C., M. C. Lu and Y. Y. Lu (2010). Distance and angle measurement of distant objects on an oblique plane based on pixel variation of CCD image. Proceeding of IEEE International Instrumentation and Measurement Technology Conference, Austin, USA, 318-322.

Kim, H., C. Lin, J. Song and H. Chae (2005). Distance measurement through a single camera and a rotating mirror. Int. J. Control, Autom., Syst. 3(4), 542-551.

Li, I-H., M. C. Chen, W. Y. Wang, S. F. Su and T. W. Lai (2014). Mobile robot self-localization system using single webcam distance measurement technology in indoor environments. sensors 14(2), 2089-2109.

Li, I-H., C. C. Hsu and S. S. Lin (2014). Map Building of Unknown Environment Based on Fuzzy Sensor Fusion of Ultrasonic Ranging Data. International Journal of Fuzzy Systems 16(3), 368-377.

Li, I-H., W. Y. Wang, Y. H. Chien and N. H. Fang (2013). Autonomous Ramp Detection and Climbing Systems for Tracked Robot Using Kinect Sensor. International Journal of Fuzzy Systems 16(3), 452-459.

Li, I-H., W. Y. Wang and C. K. Tseng (2014). A Kinect-sensor-based Tracked Robot for Exploring and Climbing Stairs. International Journal of Advanced Robotic Systems 11, 1-11.

Lee, M. F., F. H. Chiu, C. W. de Silva and C. Y. Shih (2014). Intelligent Navigation and Micro-Spectrometer Content Inspection System for a Homecare Mobile Robot. International Journal of Fuzzy Systems 16(3), 389-399.

Lu, M. C., W. Y. Wang and C. Y. Chu (2006). Image-based distance and area measuring systems. IEEE Sensors Journal 6(2), 495-503.

Nedevschi, S., R. Schmidt and T. Graf (2004). High accuracy stereo vision system for far distance obstacle detection. IEEE Intelligent Vehicles Symposium, 161-166.

Rashmi, M. Kumar and R. Saxena (2013). Algorithm and technique on various edge detection: a survey. Signal & Image Processing: An International Journal 4(3), 66-75.

Sedighi, K., K. Ashenayi, R. Wainwright and H. Tai (2004). Autonomous local path planning for a mobile robot using a genetic algorithm. IEEE

Congress on Evolutionary Computation 2, 1338-1345.

Subramanian, V., T. F. Burks and A. A. Arroyo (2006). Development of machine vision and laser radar based autonomous vehicle guidance systems for citrus grove navigation. Computers and Electronics in Agriculture 53, 130-143.

Unsalan, C. and B. Sirmacek (2012). Road Network Detection Using Probabilistic and Graph Theoretical Methods. IEEE Trans. on Geoscience and Remote Sensing 50(11), 4441-4453.

Wang, Y. and S. Fang (2009). Image-based exploration obstacle avoidance for mobile robot. Proceeding of Control and Decision Conference, 3019-3023.

Wu, S., S. Decker, P. Chang, T. Camus and J. Eledath (2009). Collision sensing by stereo vision and radar sensor fusion. IEEE Trans. on Intelligent Transportation Systems 10, 606-614.

Yasuda, G. and H. Takai (2001). Sensor-based path planning and intelligent steering control of nonholonomic mobile robots. Proceeding of Annual Conference of the IEEE Industrial Electronics Society, 317-322.

Zhao, H. and R. Shibasaki (2005). A novel system for tracking pedestrians using multiple single-row laser-range scanners. IEEE Trans. on System, Man, and Cybernetics - A: System and Humans 35(2), 283-291.

Zhu, Q., J. Hu, W. Cai and L. Henschen (2011). A new robot navigation algorithm for dynamic unknown environments based on dynamic path recomputation and an improved scout ant algorithm. Applied Soft Computing 11, 4667-4676.